AIP | Applied Physics Letters

Very large strain gauges based on single layer MoSe2 and WSe2 for sensing applications

Manouchehr Hosseini, Mohammad Elahi, Mahdi Pourfath, and David Esseni

Citation: Applied Physics Letters **107**, 253503 (2015); doi: 10.1063/1.4937438
View online: http://dx.doi.org/10.1063/1.4937438
View Table of Contents: http://scitation.aip.org/content/aip/journal/apl/107/25?ver=pdfcov
Published by the AIP Publishing

Very large strain gauges based on single layer $MoSe_2$ and WSe_2 for sensing applications

Manouchehr Hosseini,[1] Mohammad Elahi,[1] Mahdi Pourfath,[1,2,a)] and David Esseni[3]
[1]*School of Electrical and Computer Engineering, University of Tehran, North Kargar St., 14395-515 Tehran, Iran*
[2]*Institute for Microelectronics, TU Wien, Gusshausstrasse 27–29/E360, 1040 Vienna, Austria*
[3]*DIEGM, Via delle Scienze 206, 33100 Udine, Italy*

(Received 13 August 2015; accepted 26 November 2015; published online 23 December 2015)

Here, we propose a strain gauge based on single-layer $MoSe_2$ and WSe_2 and show that, in these materials, the strain induced modulation of inter-valley phonon scattering leads to large mobility changes, which in turn result in highly sensitive strain gauges. By employing density-functional theory bandstructure calculations, comprehensive scattering models, and the linearized Boltzmann equation, we explain the physical mechanisms for the high sensitivity to strain of the resistivity in single-layer $MoSe_2$ and WSe_2, discuss the reduction of the gauge factor produced by extrinsic scattering sources (e.g., chemical impurities), and propose ways to mitigate such sensitivity degradation. © *2015 AIP Publishing LLC*. [http://dx.doi.org/10.1063/1.4937438]

Strain gauge is a practical sensor with a lot of applications, such as structural health monitoring, human motion detectors, or force sensitive touch screens.[1] They are typically based on force induced changes in capacitance,[2] piezoelectricity,[3] and resistivity.[4] The advantages of resistive pressure sensors are simplicity in device fabrication as well as a relatively low energy consumption in operation. The gauge factor (GF) is a very important figure of merit for strain gauges that is defined as $GF = (\Delta R/R)/\varepsilon$, where ε is the strain magnitude, and ΔR is the corresponding resistance variation. A change in the resistance of a strain gauge is based on geometric terms and the piezo-resistive effect. The gauge factor of silicon strain gauges can reach about 100,[5] and the contribution of the piezo-resistive term is much larger than geometric terms. Due to the intrinsic stiffness, however, silicon gauges are widely used for only small strain values. Although strain gauges based on various nanomaterials, including silver nanowires ($GF \sim 1$),[6] graphene ($GF \sim 1$–3),[7] gold nanowires ($GF \sim 8$),[8] and polyethylene ($GF \sim 20$),[9] have been utilized, none has the maturity and proven effectiveness of silicon.

Two-dimensional materials with a relatively large bandgap, such as single and few-layers of transition metal dichalcogenides (TMDs), which are composed of atomic layers coupled by van der Waals forces, have been regarded as promising candidates for electronics, optoelectronics, and sensing applications.[10] We have recently shown that the mobilities of single layer (SL) MoS_2, WS_2, $MoSe_2$, and WSe_2 are strongly modulated by biaxial strain,[11,12] which stimulated us to investigate the use of TMDs as strain gauges. In this work, we present a comprehensive analysis on the effect of both biaxial and uniaxial strains on the resistivity of several TMDs, and we show that SL $MoSe_2$ and WSe_2 have extremely high strain gauge factors, which renders them excellent base-materials for sensing applications.

We have employed the density-functional theory (DFT) along with the local density approximation (LDA) as implemented in the SIESTA code to evaluate the bandstructure of SL TMDs.[13] A cutoff energy equal to 400 Ry is utilized and, by using a 30 Å vacuum region, the single layer has been isolated from other layers. The calculated lattice constants are 3.24 and 3.26 Å, respectively, for $MoSe_2$ and WSe_2, and direct bandgap energies are 1.66 and 1.72 eV, which are in agreement with previously reported values in Ref. 14. In unstrained materials, the lowest and second lowest band minima in the conduction band are denoted, respectively, as K and Q-valley (see Fig. 1). The energy distances between these valleys are evaluated to be 72 meV and 48 meV, for unstrained SL $MoSe_2$ and WSe_2, respectively. A fairly wide range of values for the energy distance between the K and Q-valley has been reported in previous theoretical studies,[14–16] and unfortunately no experimental verification has been yet reported. The 2 K-valleys are degenerate in strained and unstrained conditions. The 6 Q-valleys are also degenerate in unstrained and under biaxial strain conditions, while under uniaxial strain they split into 4 Q_A-valleys and 2 Q_B-valleys with different effective masses and energy minima. The angle θ defined in Fig. 1(e) describes the orientation of the Q-valleys in k-space. It should be noted that the zigzag direction in k-space corresponds to the armchair direction in real space. The angle θ has a very week dependence on strain, and it is approximately zero for two of the Q-valleys, $\pi/3$ for other two of them, and $2\pi/3$ for the remaining Q-valleys.

In our calculations, carrier scattering due to intrinsic phonons (both intra and inter-valley phonons), remote or surface-optical (SO) phonons, and charged impurities are taken into account. There are 6 Q-valleys in the first Brillouin zone, and phonon assisted inter-valley transitions correspond to quite different phonon wave vectors. The phonon wave vectors for inter-valley transitions are shown in Figs. 1(f)–1(h), and in all calculations we have employed the deformation potentials and phonon energies from Ref. 17.

a)Electronic addresses: pourfath@ut.ac.ir and pourfath@iue.tuwien.ac.at

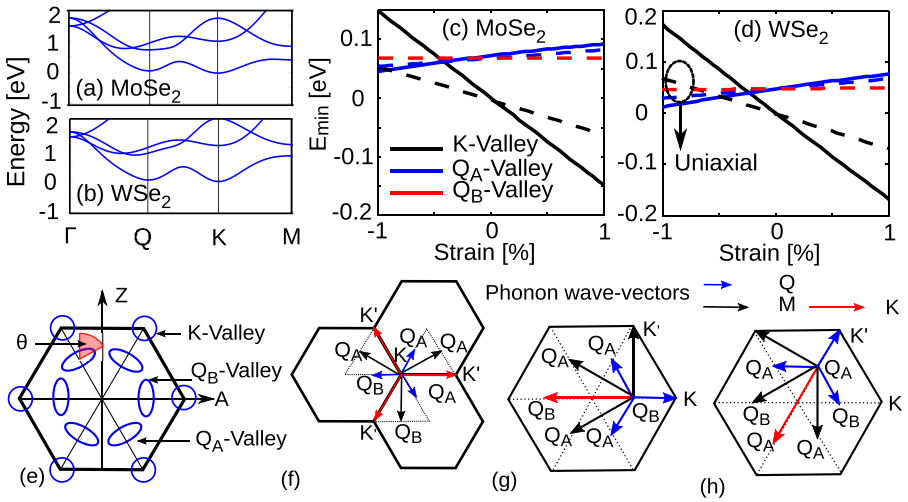

FIG. 1. The conduction band along high symmetry lines of unstrained SL: (a) $MoSe_2$ and (b) WSe_2. K is the lowest and Q is the second lowest valley in conduction band. The energy minima of K and Q-valleys of: (c) $MoSe_2$ and (d) $MoSe_2$ under biaxial strain (solid) and uniaxial strain along the armchair direction (dashed). The minimum of the K-valley in the absence of strain is taken as the zero energy reference. (e) K and Q-valleys in the first Brillouin zone of TMDs. The angle θ describes the Q-valleys orientation in $\vec{k}$-space. It should be noted that the zigzag (Z) direction in $\vec{k}$-space corresponds to the armchair (A) direction in real space. The figure also reports the illustration of several phonon assisted inter-valley transitions in SL $MoSe_2$ and WSe_2 for transitions from: (f) K-valley, (g) Q_A-valley to other valleys, and (h) Q_B-valley to other valleys.

SO phonons are another important scattering source produced by the polar phonon modes of the surrounding dielectrics. This scattering mechanism is described by assuming semi-infinite oxides and neglecting possible coupling to the plasmons of the two-dimensional (2D) material.[18] Scattering with SO phonon mode is inelastic, and we consider only intra-valley transitions.[11] Scattering with charged impurities located in the center of the 2D material has also been considered in our calculations and treated in terms of intra-valley transitions. The effect of static screening produced by the electrons in the conduction band is described by using the dielectric function approach.[19] Screening is employed for both Coulomb and SO phonons scattering, while intrinsic phonon transitions are assumed unscreened.[11]

As shown in Fig. 1(e), the bandstructure close to Q-valley is anisotropic, and the corresponding mobility shows direction-dependence, whereas the bandstructure close to K-valley is essentially isotropic. In our mobility calculations, we employed a non-parabolic energy model $E(1+\alpha E) = [\hbar^2 k_t^2/2m_t + \hbar^2 k_l^2/2m_l]$, with m_l, m_t, and α being, respectively, the longitudinal, transverse mass, and the non-parabolicity factor, that we extracted from the DFT-calculated electronic bandstructure and are reported in Table I. The longitudinal direction of Q-valleys is neither the armchair nor the zigzag direction. Therefore, an angle θ is introduced to describe the orientation of each valley, v, with respect to the armchair direction in real space (see Fig. 1(e)). The mobility of each valley along the armchair direction is then expressed as $\mu_A^{(v)} = \mu_{ll}^{(v)} \cos^2(\theta) + \mu_{tt}^{(v)} \sin^2(\theta)$,[19] where ll and tt denote the mobility, respectively, in the longitudinal and transverse direction of the valley v. The overall mobility is obtained as the average of the mobility in different valleys weighted by the corresponding electron density and has a very weak direction dependence. The mobilities have been calculated by numerically solving the linearized Boltzmann transport equation according to the approach in Refs. 11 and 20. Then, the resistivity was defined as $\rho = 1/(qn_0\mu)$, with q and n_0 being the elementary charge and carrier concentration.

TABLE I. Energy differences between the conduction band minima corresponding to K and Q-valleys (ΔE_{K-Q}), effective masses, and non-parabolicity factors as extracted from DFT bandstructure calculations and for unstrained materials.

		K-valley		Q-valley		
Material	ΔE_{K-Q}	$m_t = m_l$	α (1/eV)	m_t	m_l	α (1/eV)
MoS_2	195	0.47	0.94	0.54	1.14	1.16
WS_2	166	0.31	0.77	0.53	0.79	0.75
$MoSe_2$	72	0.55	1.21	0.47	1.08	1.29
WSe_2	48	0.34	0.97	0.45	0.76	0.87

Figs. 1(c) and 1(d) show that a compressive strain first reduces the energy distance between Q and K valleys and then induces a crossing between the same valleys, so that Q-valleys become the most populated valleys. The crossing between Q and K valleys also results in a dramatic enhancement of the inter-valley phonon scattering. In fact, it should be recalled that, according to the phonon parameters in Ref. 17, the dominant inter-valley modes (i.e., those with the largest deformation potentials) are substantially inelastic with energies ($\hbar\omega$) ranging from approximately 25 meV to 50 meV. For such phonons, the absorption rate is much smaller than the emission rate, because the phonon number $N(\hbar\omega)$ is much smaller than 1.0. In the unstrained condition, the K-valley energy minimum is lower than the Q-valley minimum by the distance ΔE_{K-Q} reported in Table I. The electrons in the K-valley can have a transition to the Q-valley and emit a phonon only for an energy $E > (\Delta E_{K-Q} + \hbar\omega)$, so that inter-valley phonon emission does not affect mobility because it is possible only for energies well above the thermal energy $K_B T$. A transition from K to Q-valley with phonon absorption is possible for $E > (\Delta E_{K-Q} - \hbar\omega)$, but the absorption is much smaller than the emission rate. Transitions from Q to K can occur, but in unstrained conditions the Q valleys give a negligible contribution to mobility.

When strain is such that Q-valley energy minima approach and then go below K-valley minima, then $(\Delta E_{K-Q} + \hbar\omega)$ becomes smaller, so that more and more electrons in the K-valley can experience a transition to Q-valley assisted by phonon emission; this results in the mobility degradation shown in Fig. 2(a). Fig. 2(a) also shows that in the strain conditions of practical interest the overall mobility tracks very closely the behavior of the K-valley mobility, which explains why the above discussion focused on K-valleys. Fig. 2(b) illustrates the resistivity variation with strain, where the maximum sensitivity corresponds approximately to the crossing between Q and K valleys observed in Figs. 1(c) and 1(d) and Fig. 2(a). Consequently, in order to observe the maximum gauge factor for strain values around zero, the energy distance between the minima of the K and Q-valleys should be small, that occurs in $MoSe_2$ and WSe_2. As expected, the high sensitivity of mobility to strain results in large gauge factors. In particular, Fig. 2(c) shows that the SL WSe_2 exhibits a maximum gauge factor of 3000, which is much larger than the gauge factor of many other materials already used or recently proposed for strain gauges. In MoS_2 and WS_2, however, the energy differences between the minima of the K and Q-valley are relatively large, which results in small gauge factors for strain values close to zero. To enhance the gauge factor for these two materials, a mechanical strain offset can be applied, but this may not be practical for some applications.

An ideal TMD is free from dangling bonds and defects; however, during the exfoliation or growth processes, imperfections can be unintentionally produced.[21] Defects and the oxidation of the surface can affect the bandgap[22–24] and induce localized states and traps in the middle of the gap.[21,25] The variation of the bandgap, however, is not expected to affect our predicted results as long as it does not change the energy distance between K and Q minima in the conduction band. A careful analysis of the role of defects requires atomistic simulations, and it is beyond the scope of this work.

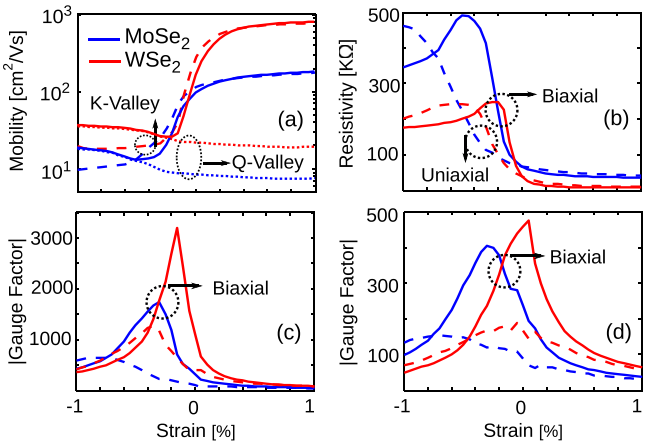

FIG. 2. (a) The phonon limited mobility as a function of strain: overall mobility (solid), mobility in K-valleys (dashed), and mobility in Q-valleys (dotted). (b) The resistivities; (c) and (d) the gauge factors as functions of strain. Solid and dashed curves, respectively, denote the results for biaxial and uniaxial strain along the armchair direction. (b) and (c) correspond to results including only intrinsic phonon scattering; results in (d), instead, account for intrinsic phonon, remote phonon, and charge impurity scattering. Top and back oxides are assumed to be SiO_2. The impurity and carrier concentrations are $10^{11}\,cm^{-2}$ and $10^{12}\,cm^{-2}$, respectively.

Scattering with charged impurities and remote phonon induces intra-valley transitions, which are only weakly affected by strain. Consequently, the strain gauge is reduced when such extrinsic scattering mechanisms are included, as illustrated in Fig. 2(d). In this latter respect, Fig. 3(a) shows the gauge factors of SL WSe_2 and $MoSe_2$ are degraded as intra-valley transitions due to charged impurities become dominant. The scattering due to charged impurities, however, can be significantly reduced by the screening produced by the free electrons, whose concentration in 2D materials can be modulated using an electrostatic doping.[10] This is confirmed by Fig. 3(b) showing that, for a given impurity concentration, the gauge factor increases with the carrier concentration. Similarly, the impurity scattering may also be reduced thanks to the dielectric screening produced by the surrounding dielectrics.[11] In this respect, Fig. 3(c) shows that the gauge factor first increases with the relative dielectric constant κ of the gate oxide, but then it reduces again, because in materials with higher κ the corresponding smaller SO phonon energies enhance the SO phonons scattering, which is intra-valley (just as charged impurity scattering) and thus less sensitive to strain compared to inter-valley scattering.

Finally, the temperature dependence of the gauge factor is investigated. Fig. 3(d) indicates that at low temperatures the gauge factor is rather small because of the corresponding reduced inter-valley phonon transitions and, furthermore, it increases with the temperature following the relative importance of inter-valley phonons in determining the overall mobility. At temperatures above 200 K, however, the gauge factor of WSe_2 starts to decrease as the temperature increases. This behavior is due to increased contribution of the Q-valley, which has a weaker effective mass variation and correspondingly a smaller resistivity modulation with strain in comparison with that of K-valley. Thus, at temperatures above

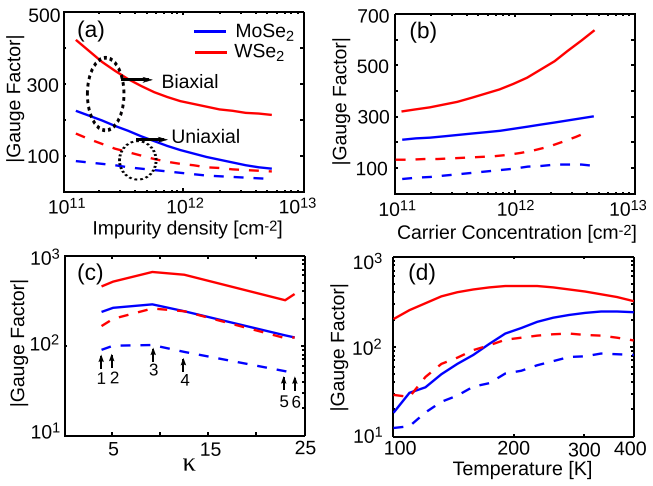

FIG. 3. The gauge factor versus (a) charged impurity concentration at a carrier concentration of 10^{12} cm^2 and (b) carrier concentration at a charged impurity density of 10^{11} cm^2 ($T = 300$ K). (c) The gauge factor for various top oxide materials. κ is the dielectric constant, and the numbers 1 to 6 represent the dielectric materials studied in this work. In particular, (1): SiO_2, (2): BN, (3): AlN, (4): Al_2O_3, (5): HfO_2, and (6): ZrO_2. In all the cases, the back oxide is assumed to be SiO_2. (d) The gauge factor versus temperature. In all of the cases, scattering from intrinsic phonons, screened remote phonons, and screened charged impurities have been included. In (c) and (d), the impurity and carrier concentrations are equal to 10^{11} cm^{-2} and 10^{12} cm^{-2}, respectively.

200 K, the gauge factor is slightly reduced as temperature increases. Because of a higher energy distance between the K and Q-valleys, this behavior is not observed in SL $MoSe_2$.

In our bandstructure calculations, the effect of spin orbit coupling (SOC) has been neglected. The SOC splittings (Δ_{SO}) in the conduction band of $MoSe_2$ at the K and Q valley minima are relatively small, and their effect on the resistivity is expected to be minimal, whereas this splitting is larger in WSe_2, especially close to Q-valley minimum. At the time of writing, it is unfortunately difficult to have a dependable estimate of SOC splittings, in fact DFT calculations predicted different values up to 40 meV and 220 meV, respectively, close to the K and Q minimum of WSe_2,[16,26,27] while no experimental verification has yet been reported. By considering SOC splitting, the strain induced variation of inter-valley phonon assisted scattering rates is reduced, which in turn results in a degradation of the strain gauge factor. Therefore, we believe that, for WSe_2, the results in our work indicate the upper limit of the gauge factor, and a degradation is expected depending on the exact value of the SOC splitting. This degradation, however, should be relatively small when significant intra-valley transitions are present, such as scattering with Coulomb charges and remote phonons of the surrendering dielectrics.

In summary, we propose SL WSe_2 and $MoSe_2$ as excellent base materials for highly sensitive strain gauges. Unlike conventional strain gauges where geometric and piezoelectric terms contribute to the gauge factor, in these materials, it is the inter-valley phonon limited mobility which is strongly affected by strain and thus results in large gauge factors. Even in the presence of extrinsic scattering sources, the gauge factors of these materials are much larger than those reported for most of the materials typically used for strain gauges. By using a gated structure, the charged impurities can be partly screened, which can effectively contrast the Coulomb scattering induced reduction of the gauge factors.

This work has been partly supported by the Iran National Science Foundation (INSF) under Grant No. 93038367.

[1]G. Schwartz, B. C.-K. Tee, J. Mei, A. L. Appleton, D. H. Kim, H. Wang, and Z. Bao, Nat. Commun. **4**, 1859 (2013).
[2]D. J. Cohen, D. Mitra, K. Peterson, and M. M. Maharbiz, Nano Lett. **12**, 1821 (2012).
[3]Q. Gao, H. Meguro, S. Okamoto, and M. Kimura, Langmuir **28**, 17593 (2012).
[4]T. Yamada, Y. Hayamizu, Y. Yamamoto, Y. Yomogida, A. Izadi-Najafabadi, D. N. Futaba, and K. Hata, Nat. Nanotechnol. **6**, 296 (2011).
[5]V. Mosser, J. Suski, J. Goss, and E. Obermeier, Sens. Actuators, A **28**, 113 (1991).
[6]W. Hu, X. Niu, R. Zhao, and Q. Pei, Appl. Phys. Lett. **102**, 083303 (2013).
[7]A. Smith, F. Niklaus, A. Paussa, S. Vaziri, A. C. Fischer, M. Sterner, F. Forsberg, A. Delin, D. Esseni, P. Palestri *et al.*, Nano Lett. **13**, 3237 (2013).
[8]S. Gong, W. Schwalb, Y. Wang, Y. Chen, Y. Tang, J. Si, B. Shirinzadeh, and W. Cheng, Nat. Commun. **5**, 3132 (2014).
[9]N. Olichwer, E. W. Leib, A. H. Halfar, A. Petrov, and T. Vossmeyer, ACS Appl. Mater. Interfaces **4**, 6151 (2012).
[10]B. Radisavljevic and A. Kis, Nat. Mater. **12**, 815 (2013).
[11]M. Hosseini, M. Elahi, M. Pourfath, and D. Esseni, J. Phys. D: Appl. Phys. **48**, 375104 (2015).
[12]M. Hosseini, M. Elahi, M. Pourfath, and D. Esseni, IEEE Trans. Electron Devices **62**, 3192 (2015).
[13]J. M. Soler, E. Artacho, J. D. Gale, A. García, J. Junquera, P. Ordejón, and D. Sánchez-Portal, J. Phys.: Condens. Matter **14**, 2745 (2002).
[14]A. Kumar and P. Ahluwalia, Eur. J. Phys. B **85**, 186 (2012).
[15]C.-H. Chang, X. Fan, S.-H. Lin, and J.-L. Kuo, Phys. Rev. B **88**, 195420 (2013).
[16]A. Ramasubramaniam, Phys. Rev. B **86**, 115409 (2012).
[17]Z. Jin, X. Li, J. T. Mullen, and K. W. Kim, Phys. Rev. B **90**, 045422 (2014).
[18]Z.-Y. Ong and M. V. Fischetti, Phys. Rev. B **88**, 045405 (2013).
[19]D. Esseni, P. Palestri, and L. Selmi, *Nanoscale MOS Transistors* (Cambridge University Press, Cambridge, 2011).
[20]A. Paussa and D. Esseni, J. Appl. Phys. **113**, 093702 (2013).
[21]W. Zhou, X. Zou, S. Najmaei, Z. Liu, Y. Shi, J. Kong, J. Lou, P. M. Ajayan, B. I. Yakobson, and J.-C. Idrobo, Nano Lett. **13**, 2615 (2013).
[22]K. Santosh, R. C. Longo, R. Addou, R. M. Wallace, and K. Cho, Nanotechnology **25**, 375703 (2014).
[23]K. Santosh, R. C. Longo, R. M. Wallace, and K. Cho, J. Appl. Phys. **117**, 135301 (2015).
[24]H.-P. Komsa and A. V. Krasheninnikov, Phys. Rev. B **91**, 125304 (2015).
[25]H. Qiu, T. Xu, Z. Wang, W. Ren, H. Nan, Z. Ni, Q. Chen, S. Yuan, F. Miao, F. Song *et al.*, Nat. Commun. **4**, 2642 (2013).
[26]D. Wickramaratne, F. Zahid, and R. K. Lake, J. Chem. Phys. **140**, 124710 (2014).
[27]A. Kormanyos, G. Burkard, M. Gmitra, J. Fabian, V. Zolyomi, N. D. Drummond, and V. Fal'ko, 2D Mater. **2**, 022001 (2015).